ACS Sustainable Chemistry & Engineering

Research Article

pubs.acs.org/journal/ascecg

The Physicochemistry of Capped Nanosilver Predicts Its Biological Activity in Rat Brain Endothelial Cells (RBEC4)

Bellina Veronesi,*[,†] Brian Chorley,[†] William Ward,[‡] Steven O. Simmons,[†] Alan Tennant,[†] and Beena Vallanat[‡]

[†]National Health and Environmental Effects Research Laboratory (Integrated Systems Toxicology Division) and [‡]Genomics Research Core, U.S. Environmental Protection Agency, Research Triangle Park, North Carolina 27711, United States

Supporting Information

ABSTRACT: The "capping" or coating of nanosilver (nanoAg) extends its potency by limiting its oxidation and aggregation and stabilizing its size and shape. The ability of such coated nanoAg to alter the permeability and activate oxidative stress pathways in rat brain endothelial cells (RBEC4) was examined in the present study. The aggregate size and zeta potential of nanoAg with different sizes (10 and 75 nm) and coatings (PVP and citrate) were measured in cell culture media. Results indicated that both PVP-coated nanoAg were less electronegative than their citrate-coated counterparts over all exposure times, but only the PVP-coated 10 nm particles retained their initial electronegativity over all exposure times. In addition, only the PVP-coated particles retained their initial sizes throughout the 3 h measurement. PVP-coated 10 nm nanoAg selectively altered the permeability of RBEC4 monolayers within a 15 min exposure, although high resolution microscopy indicated that all coated nanoAg distributed throughout the cell's cytoplasm within the 3 h exposure. Reporter genes for AP-1 and NRF2/ARE, transfected into RBEC4, were selectively stimulated by the PVP-coated 10 nm nanoAg. Global gene arrays indicated that only PVP-coated nanoAg significantly altered gene expressions in the RBEC4, and those altered by 10 nm PVP-coated nanoAg were qualitatively similar but quantitatively much higher than those of its 75 nm counterpart. IPA and DAVID analyses indicated that the altered pathways affected by both PVP-coated nanoAg were primarily associated with a NRF2-mediated oxidative stress response, endocytosis, and bioenergetics. Together, these data suggest that the physicochemical features of surface coating aggregate size and surface charge contribute to capped nanoAg's permeability and oxidative stress responses in RBEC4.

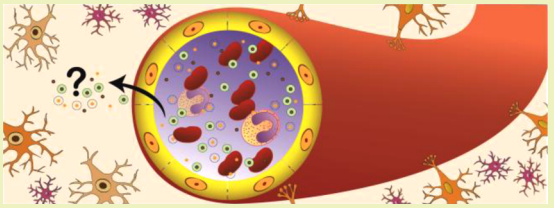

KEYWORDS: *Sustainability, Nanosilver, Surface coating, Capping, Nanotoxicity, RBEC4, Blood brain barrier permeability, Transcellular resistance, Oxidative stress, Polyvinylpyrrolidone, PVP, Citrate, Physicochemistry, Endocytosis, NRF2, Vegfa, Slc1a2*

INTRODUCTION

Nanosilver (nanoAg) is used in a variety of industrial and consumer products (e.g., textiles, paints, electronics, biosensors, water disinfectant, household appliances, food packaging, detergents, air and water filters, toothpaste, sunscreens, lotions, cosmetics, etc.).[1−4] Because of its antimicrobial activity, nanoAg is also found in medical products (e.g., antiseptics, dressings for external wounds and skin burns, embedded medical devices, etc.)[5,6] and is currently listed in over 53% of EPA-registered biocidal products.[7] Surface coating or "capping" is done to limit its oxidation,[8] aggregation, ionic release, and stabilize its size and shape,[9] thereby sustaining its effectiveness. The most common stabilizing agents are citrate[10] and the polymer polyvinylpyrrolidone (PVP).[11] A 2010 review of the scientific literature indicates that both are the most common coatings used to stabilize the nanoAg found in commercial and environmental applications.[12] Although the formulations of environmentally relevant products using PVP and citrate coatings are protected by confidential protection information (CBI), both coatings are currently used in roofing shingles, solar cells coatings, clothing, hand sanitizers, and forestry products (S. Oldenberg, nanoComposix, Inc., San Diego, CA, personal communications).

Because of their widespread use in environmental, medical, and consumer products, these coated nanoAg materials can be expected to encounter multiple biological systems and damage vulnerable systems. One potential target is the mammalian brain, given its extreme sensitivity to oxidative stress damage[13−16] and nanoAg's association with oxidative stress.[17−21] To pose neurotoxic risk, however, nanoAg must pass through the highly restrictive blood brain barrier (BBB), which is characterized by tight junctions, high electrical resistance, multiple metabolic enzymes, and efflux transport systems.[22,23] In vitro models of the BBB have been developed that contain these essential characteristics and are increasingly used to study its permeability and transport systems. One successful model is RBEC4, an immortalized rat brain endothelial cell line[24] that shows low but measurable and responsive levels of the receptors, enzymes, intercellular adhesion molecules, and transporter systems such as

Special Issue: Sustainable Nanotechnology 2013

Received: February 11, 2014
Revised: April 8, 2014
Published: April 23, 2014

expression of P-glycoprotein, occludin, and ZO-1. Although lacking the extreme paracellular impermeability of BBB in situ, these cells do form intact high resistance monolayers, house functional tight junctions, and have been used to study drug permeability[25−28] and that associated with nanoparticle exposure.[24,29−31] Because several studies indicate PVP-capped[32] or uncapped[1,33] nanoAg distributes to the brain and other organs of rats and mice, this in vitro model was used to examine the response of brain endothelial cells to nanoAg.

Linking the physical properties of nanoparticles with differences in their biological activity is critical for understanding their mode of action and potential toxicity. Most importantly, such information helps in the design of safe, cost-effective, and more sustainable nanomaterials. This study adds to this literature by using the RBEC4 barrier model to examine if nanoAg of different sizes (10 and 75 nm) and coatings (citrate and PVP) differentially alters their permeability and cellular and genomic responses.

MATERIALS AND METHODS

Test Substances. NanoAg of different sizes (10 and 75 nm) and coatings (PVP and citrate) were purchased as 1 mg/mL suspensions in their respective vehicle (i.e., distilled water, 0.2 mM sodium citrate) by nanoComposix, Inc., San Diego, CA. Chemical analysis was performed by the manufacturer (nanoComposix.com/product-silver/biopure-silver.html) and reported to be 99.8% pure. A variety of techniques were used to measure the response of RBEC4 at various times and concentrations. These included basic physicochemical measures (aggregate size and surface charge) in exposure media over several time points; high resolution microscopy (confocal, electron microscopy) to examine their translocation of the RBEC4; permeability measures in RBEC4 monolayers using transcellular electrical resistance (TER) recordings; fluorescence-based viability and oxidative stress assays; and genomic evaluation using transfected reporter genes, target gene expression, and global gene expression. All techniques are fully described in the Supporting Information.

RESULTS

Physicochemistry (PC). PC measurements (i.e., aggregate size, surface charge) of each coated nanoAg (10−20 ppm suspensions) were collected in RBEC4 media at time points that bracketed the TER (T = 10 min) and morphological (T = 1 h, 3 h) exposures. At T = 10 min, both the 10 nm (−13.48 mV) and 75 nm (−11.6 mV) PVP-coated nanoAg were less negative than their citrate-coated counterparts (10 nm −20.77 mV; 75 nm −15.33 mV), but only the PVP-coated 10 nm particles retained this electronegativity over all exposure times. Measures of the aggregate size of each material, presented as the peak mean >90%, indicated that only PVP-coated nanoAg retained its initial size throughout the 3 h measurement time (Table S1, Supporting Information). Efforts to measure at 18 h failed due to particle sedimentation. Data were analyzed using a one-way ANOVA followed by a Tukey's posthoc analysis.

Transcellular Electrical Resistance (TER). RBEC4 monolayers, grown in Millicell 96 well plates, were first measured for baseline resistance (T = 0), and only those showing stable recordings ≥200 Ohm were used for testing. For this, wells were exposed to noncytotoxic (6.5 ppm) concentrations of each nanoAg material suspended by ultrasonication in RBEC4 culture media. Readings (Ohm) were converted by REMS software into TER units. Significant changes in stable resistance occurred after 15 and 30 min exposure to PVP-coated 10 nm nanoAg (Figure 1), after which time the measures were stopped to avoid any artifactual responses resulting from the cultures being held outside of incubator conditions (5% CO_2; 37 °C). Treatment values were normalized to their T = 0 baseline values and statistically analyzed using a one-way ANOVA, followed by Dunnett's multiple comparison test.

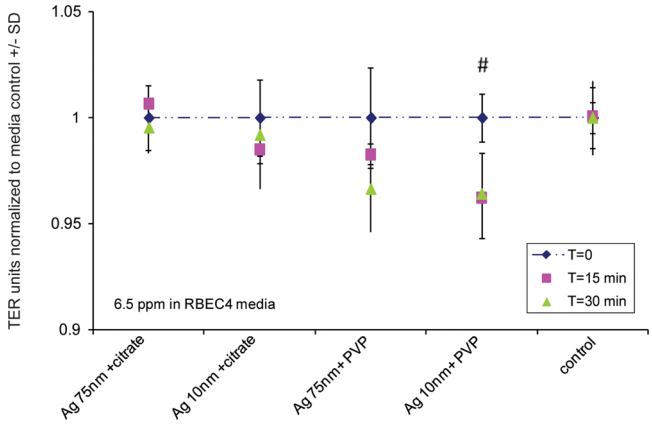

Figure 1. Transcellular electrical resistance (TER) was used to measure alterations of membrane permeability in RBEC4 monolayers. Resistance measures indicated that 6.5 ppm of 10 nm PVP-coated nanoAg significantly altered the permeability of the monolayers after 15−30 min exposure. TER units were averaged (n = 6 well/treatment) and normalized to their T = 0 value at each time point. There was no significant difference in the response of the citrate or distilled water vehicle + media controls, and their values were combined and presented as the control. Data were statistically analyzed using a one-way ANOVA, followed by Dunnett's multiple comparison test and are presented ± SD. Significance (p-value < 0.05) is indicated.

Morphology. Nonconfluent RBEC4, exposed for 1 h to 6.5 ppm of each material, were examined by fluorescence and differential interference contrast (DIC) microscopy. By fluorescence, Mitotracker stained red mitochondria and DAPI stained bluish nuclei stood in sharp contrast to the cytoplasmic green nanoAg aggregates that resonate in the FITC wavelength range (Figure 2A). Confocal Z-stack images of cells exposed to each material indicated that the aggregates distributed throughout the cell cytoplasm after 0.5−1 h exposure to 10 nm PVP-coated nanoAg and for all nanoAg samples within a 3 h exposure time. Particles were noted below the plane of DAPI stained nuclei (Figure 2B, circles), indicating that the nanoAg particles physically entered the RBEC4 cytoplasm. TEM of confluent RBEC4 exposed to 6.5 ppm nanoAg for 3 h indicated that nanoAg aggregates could be seen through the cytoplasm with smaller size aggregates lodged into the mitochondria. In all instances, tight junctions of RBEC4 monolayers treated with each nanoAg appeared ultrastructurally intact, in spite of morphological evidence that nanoAg aggregates distributed intracellularly (Figure 2C).

Cellular Assays. In view of the possibility that the citrate or PVP coatings could destabilize over the long exposure times and release highly toxic Ag ions (Ag+),[8,34−36] RBEC4 were exposed for 18 h to Ag^+ in the form of silver nitrate ($AgNO_3$) (0.8−100 ppm) suspended in cell culture media. Results indicated that cytotoxicity only occurred at concentrations ≥12.5 ppm (Figure S1, Supporting Information). This experiment, and studies by Kittler et al.,[37] which suggest that serum found in the cell culture media can bind released Ag^+ and reduce the toxicity of coated nanoAg, offered assurance that the cellular effects of coated nanoAgs (which were exposed at much lower concentrations and shorter time points) were unrelated to cellular perturbations associated with Ag^+. Cytotoxicity assays were next conducted on

dx.doi.org/10.1021/sc5000896 | ACS Sustainable Chem. Eng. 2014, 2, 1566−1573

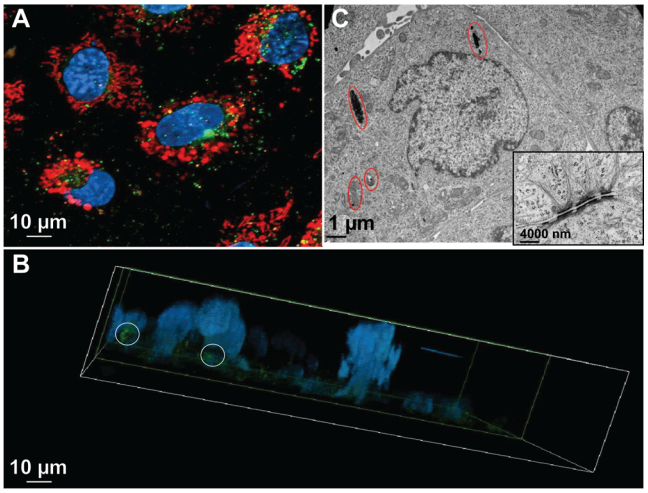

Figure 2. Nonconfluent RBEC4 were exposed to 6.5 ppm of nanoAg 10 nm + PVP for 1 h and examined by fluorescent microscopy using a 60× oil immersion lens (A). The Mitotracker red stain of viable mitochondria stain and the bluish nuclear stain of DAPI appeared in sharp contrast to the FITC resonance of the nanoAg aggregates. Confocal Z-stacks demonstrated the intracytoplasmic distribution of the nanoAg particles in exposed RBEC4 (B). NanoAg aggregates could be seen dispersed throughout the cell cytoplasm and below the DAPI stained nuclei (B, circles), indicating that nanoAg particles had translocated the RBEC4. PVP-coated 10 nm particles were the first to be detected 1 h; however, by 3 h exposure, each particle sample appeared distributed throughout the cytoplasm. TEM of RBEC4 exposed to 6.5 ppm nanoAg for 3 h indicated small aggregates of nanoAg could be seen distributed through the cytoplasm (circles). Smaller size aggregates appeared within the mitochondria (circles) (C). In all instances, the cell's tight junctions appeared ultrastructurally intact (insert).

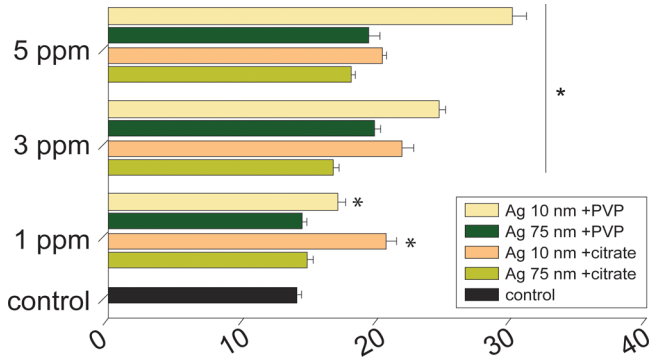

Figure 3. Noncytotoxic concentrations of each nanoAg (1−5 ppm) were exposed to semi-confluent RBEC4 for 18 h and examined for caspase 3/7 activity as a measure of apoptosis. All nanoAg samples (>3 ppm) stimulated activity but only the 10 nm nanoAg, coated with either PVP or citrate, stimulated caspase 3/7 activity at all concentrations (>1 ppm). There was no significant difference in the response of the citrate or distilled water vehicle + media controls. Their values are combined and presented as the control. Chemiluminescent units, collected at 3 s integration are given on the X axis. Data were statistically analyzed using a one-way ANOVA, followed by Dunnett's multiple comparison test and are presented ± SD. Significance (p-value < 0.05) is indicated with asterisks.

semi-confluent RBEC4 exposed to each coated nanoAg (0.5−7 ppm) for 18 h. No significant change in intracellular ATP levels as assessed by CellTiter-Glo viability assays was noted at any test concentration (data not shown). On the basis of these data, noncytotoxic concentrations of nanoAg (1−5 ppm) were exposed to semi-confluent RBEC4 for 18 h and assayed for caspase 3/7 activity, an index of apoptosis. Results indicated that all nanoAg samples (≥3 ppm) stimulated activity, but only the 10 nm nanoAg coated with either PVP or citrate stimulated caspase 3/7 activity at the lowest test concentration (≥1.0 ppm) (Figure 3).

Reporter Genes. Noncytotoxic (1−4 ppm) concentrations of each coated nanoAg were exposed for 18 h to semi-confluent RBEC4 in culture media. Controls consisted of culture media with 10% concentrations of either distilled water or 0.2 mM citrate buffer to parallel their exposure conditions. Results indicated that both sizes of PVP-coated nanoAg stimulated AP-1 reporter gene activity, but only the 10 nm PVP-coated nanoAg stimulated NRF2/ARE reporter gene activity at all concentrations (Figure 4A,B).

NRF2 Target Gene Expression. Levels of the NRF2 target genes *Gsta3* and *Nqo1* were measured after exposure to each nanoAg at the lowest effective concentration (1.0 ppm) for 4, 8, and 18 h. Although, no significant changes were seen with the *Nqo1* expression at any exposure time (data not shown), the *Gsta3* expression was significantly increased over all time points by 10 nm PVP-coated nanoAg and after 18 h exposure in response to the 75 nm PVP material. Both sizes of citrate-coated nanoAg only gave marginal responses at 18 h (Figure 5). Given that the 18 h exposure gave the maximum response for the *Gsta3* target gene expression and both reporter genes, this time point was used to measure global gene expression.

Global Gene Expression. Principal component (PCA) of the quantile-normalized probe data showed the number of genes stimulated by the PVP-coated nanoAg differed significantly from their media controls and their citrate-coated counterparts. However, PVP-coated 10 nm nanoAg produced the most robust changes, relative to the others as shown by the gene expression variance along the first principal component (Figure 6A). Compared to controls, 10 nm PVP-coated nanoAg significantly altered 928 genes (428/500 up/down) relative to 68 genes (32/36 up/down) by the 75 nm PVP-coated nanoAg. A gene list comparison indicated that 66/68 of these genes were shared and in the same direction as the PVP-coated nanoAg 10 nm (Figure 6B). Only two altered genes were unique to the 75 nm PVP-coated nanoAg, those being *Cdc40* (cell division cycle 40) and *Hnrnpf* (heterogeneous nuclear ribonucleoprotein F). Because 66/68 genes of these genes were shared by the PVP-coated 10 nm material, both IPA and DAVID (signaling pathway and cellular function) analyses focused on gene changes associated with the 10 nm PVP-coated nanoAg exposure. IPA analysis indicated that gene changes caused by the PVP-coated 10 nm material were associated with enzymatic, transcription regulation, kinase, transporter, peptidase, and phosphatase functions (Figure S2, Supporting Information). Canonical pathways and toxicity lists enriched by these genes included NRF2-mediated oxidative stress response, protein ubiquitination, nuclear receptor-mediated, and CNS-centric ephrin pathway signaling. Of all significantly changed genes (408 genes), IPA canonical pathway and toxicity list enrichment analyses produced a similar but shorter list, where the most significant pathways were specifically associated with the NRF2 oxidative stress and protein ubiquitination pathways (Bonferroni−Hochberg adjusted p-value < 0.05) (Table S2, Supporting Information). DAVID-reflected enrichment analysis indicated a functional annotation clustering of all PVP-coated 75 nm nanoAg altered genes indicating that processes such as protein catabolism, ubiquitination, gene expression regulation, and neuronal differentiation and

dx.doi.org/10.1021/sc5000896 | ACS Sustainable Chem. Eng. 2014, 2, 1566−1573

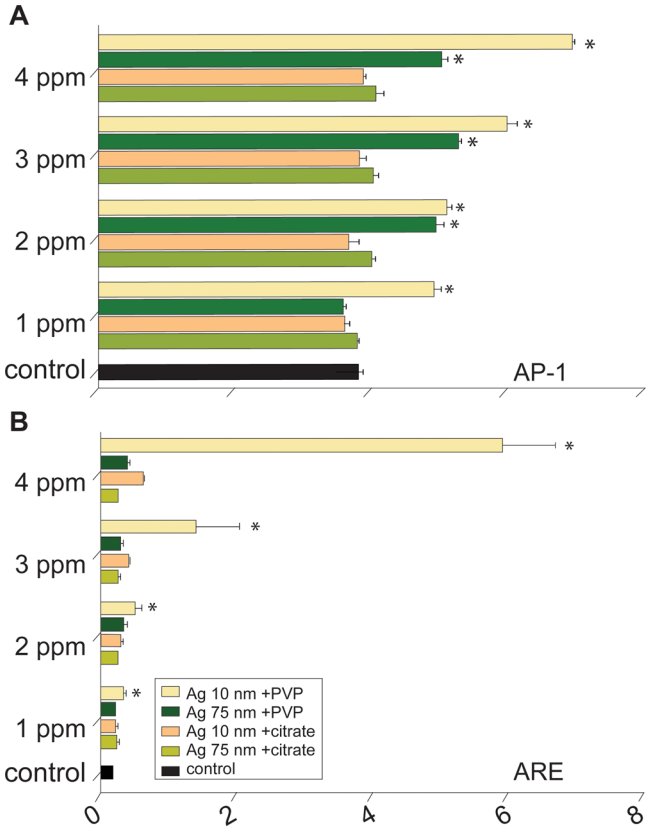

Figure 4. Activation of reporter genes was examined in RBEC4 exposed to each nanoAg material (1−4 ppm) for 18 h. Only PVP-coated nanoAg of both sizes stimulated AP-1 (A), but only the 10 nm PVP-coated nanoAg stimulated NRF2/ARE activity at all concentrations (B). There was no significant difference in the response of the citrate or distilled water vehicle + media controls, and their values were combined and presented as the control. Chemiluminescent units, collected after 3 s integration, are represented on the X axis. Data were statistically analyzed using a one-way ANOVA, followed by Dunnett's multiple comparison test and are presented ± SD. Significance (p-value < 0.05) is indicated with asterisks.

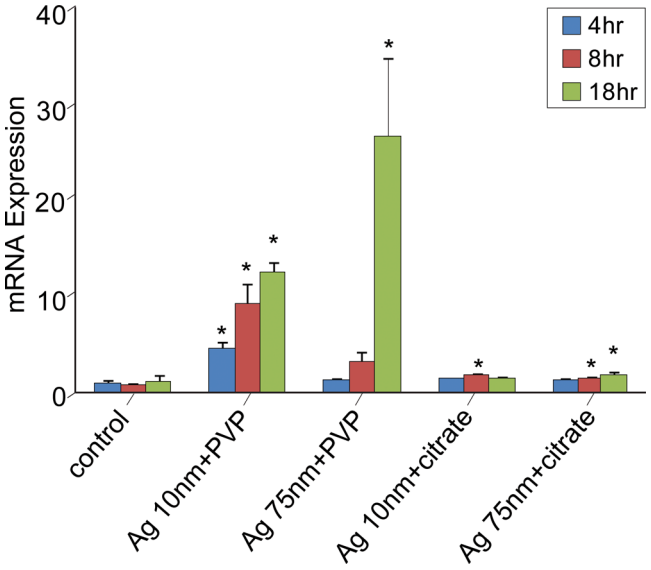

Figure 5. NanoAg treatment upregulated the expression of the NRF2 target gene, *Gsta3*, in RBEC4 exposed to 1.0 ppm for 4, 8, and 18 h. Although all materials were able to stimulate this target gene of NRF2 activity, only 10 nm PVP-nanoAg significantly increased *Gsta3* expression at all time points in a dose−response fashion. Bars represent fold changes relative to respective controls. Data were statistically analyzed using Student's t test, and significance (p-value < 0.05) is indicated by asterisks.

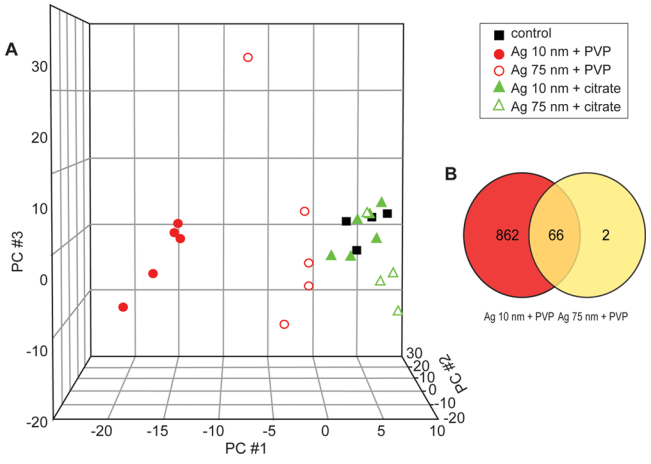

Figure 6. PCA of all expressed genes indicated that both sizes of PVP−nanoAg treatments were significantly distinct from their respective controls (not significantly different and combined for graphing purposes) and their citrate-coated counterparts. PVP-coated nanoAg 10 nm significantly altered 928 genes (428/500 up/down) relative to the 68 genes (32/36 up/down) associated with PVP-coated Ag 75 nm nanoAg (A). A gene list comparison of the latter changes demonstrated that 66 of these 68 genes were shared and in the same direction as the 10 nm PVP-coated nanoAg (B). Significantly altered genes were defined by Bayesian t test with multiple test correction using the Benjamini−Hochberg method at an alpha of 0.05.

development were similarly affected (Table S3, Supporting Information). IPA also indicated an activation of NRF2 and interferon gamma and an inhibition of gene expression regulators, insulin-like growth factor 1 receptor, and the insulin receptors CREB, beta catenin, and PPAR gamma (Table S4, Supporting Information). In addition to the oxidative stress response, PVP-coated 10 nm nanoAg exposure altered expression of genes linked to BBB function including clathrin-mediated endocytosis (*Clta*, *Cltc*, *Ap1s2*, *Ap2s1*), caveolar invagination (*Cav1*), and vesicle trafficking (*Sec24d*). The solute carrier family of proteins (*Slc1a2*), a high affinity glutamate transporter,[38] was the highest upregulated gene in response to both the 10 nm (7.64 fold) and 75 nm (4.6 fold) PVP-coated nanoAg and the only gene significantly altered (1.84 fold) by 10 nm citrate-coated nanoAg. Vascular endothelial growth factor (*Vegfa*) was marginally but significantly increased by both 10 nm (1.8 fold) and 75 nm (1.6 fold) of the PVP-coated material. All microarray data were deposited in the Gene Expression Omnibus with accession number GSE47543.

DISCUSSION

The influence of nanoAg's size, surface coating, and surface charge was examined in the present study. The results indicate that a combination of coating (PVP) and small size was most influential in altering membrane permeability and stimulating an oxidative stress response in RBEC4. Permeability changes, as measured by TER resistance, were most rapid (15 min) for the 10 nm PVP-coated material. However, this permeabilty was not selective because high resolution microscopy showed that all nanoAg entered the RBEC4 after longer (3 h) exposures. This

dx.doi.org/10.1021/sc5000896 | ACS Sustainable Chem. Eng. 2014, 2, 1566−1573

translocation was rapid and occurred in the absence of tight junctional disruption, as reported by others.[39−41] Genomically, PVP-coated 10 nm nanoAg produced greater cellular and genomic changes than the other tested materials, and these changes were largely associated with NRF2 oxidative stress pathways.

The purpose of this study was to determine if a linkage could be demonstrated between these cellular responses and key physicochemical features of the coated nanoAg. A growing list of physicochemical features (e.g., surface charge, size, surface area, electrophoretic mobility, surface coatings, topography, pore volume, crystalline structure, lipophilicity, etc.) has been linked to the biological activity (e.g., cellular uptake, cellular motility, redox activity cellular communication) and toxicity[42−49] of nanomaterials. In our study, the less affected zeta potential of the 10 nm PVP-coated nanoAg appeared more reactive to the RBEC4. Higher toxicity and the less negative surface charge of PVP-coated nanoAg relative to its citrate-coated counterpart have been reported by others.[47] The smaller size of the PVP-coated 10 nm nanoAg also influenced its bioreactivity possibly by facilitating the particle's cellular uptake and transcellular movement and providing a closer proximity to those enzymatic and bioenergetic sites (e.g., mitochondria) associated with oxidative stress, as has been suggested for ultrafine airborn pollutants.[50−52]

More than size and charge, however, the PVP surface coating appeared to play an influential role in its higher bioreactivity. Coating the nanoAg is known to reduce its oxidation, preserve its size, and reduce its toxicity. Coating with PVP polymer provides a more stable nanoAg than citrate yielding a stable colloidal suspension.[32,53,54] Its greater stability has been studied over a range of monovalent and divalent electrolyte concentrations outside of low pH environments.[53] The aggregate size of capped nanoAg has been studied under various ionic strengths and acidic pH conditions[54] and indicate a negligible impact of these conditions on the sterically stabilized PVP-coated nanoAg. This was also observed in the recent Caballerro−Diaz study that measured <1% release of Ag^+ after a 7 d incubation in pH 3.0 environments.[55] Together, these studies and the present data suggest that the high bioreactivity of the 10 nm PVP-coated nanoAg could relate to the size and charge stability provided by the PVP coating. It should be noted, however, that both coated materials precipitated out after 18 h, suggesting that PVP-coated materials may also be unstable under long-term physiological conditions. The genomic data underscored the higher bioreactivity of the PVP 10 nm nanoAg. The primary pathways affected involved NRF2 oxidative stress transcripts that activate to protect the cell against oxidative stress. Reporter genes indicated that both sizes of PVP-coated materials affected AP-1 reporter gene activity, but only the 10 nm nanoAg activated the NRF2/ARE reporter gene. Because multiple transcriptional and post-transcriptional mechanisms can alter NRF2 pathway activation and ultimately the upregulation of NRF2 target gene transcription,[56] two NRF2 target genes, *Nqo1* and *Gsta3*, were measured as biomarkers of increased NRF2 activity.[56,57] However, in contrast to the robust activation of *Gsta3* at all time points, *Nqo1* levels appeared unaffected. This failure to respond is unclear but might relate to its co-regulation by other transcriptional factors in the RBEC4 such as silencing epigenetic mechanisms, as reported in other cell types.[58] Another concern involved the failure of the 75 nm size PVP nanoAg to activate the ARE reporter gene (Figure 4), but its activation of *Gsta3* at 18 h (Figure 5). Although both techniques (i.e., reporter genes, qPCR) involved gene expression and focused on NRF2 transcript, they asked different questions. For example, the reporter gene addressed if PVP exposure activated the transcription factor of interest (ARE, AP-1), and qPCR examined if PVP exposure affected the expression of the *Gsta3* gene. In addition, reporter assays rely on protein-level responses (i.e., luciferase, GFP, etc.), which are preceded in time by mRNA. In contrast, RT/qPCR looks at mRNA/cDNA levels and not protein. Even though both focused on the same transcript NRF2, mRNA increases preceded protein levels increases and could be detected earlier. In addition, it is unlikely to expect that the luciferase mRNA and protein would have the same stability or kinetics as *Gsta3* mRNA.

The global microarray data indicated that PVP-coated nanoAg activated an ARE/NRF2-mediated protective response against oxidative stress. NRF2 is a transcriptional factor that binds to the antioxidant response element ARE and regulates a battery of gene expressions involved in cellular antioxidant and anti-inflammatory defense.[59] Its activation by the PVP-coated nanoAg should be viewed as a major protection response by the RBEC4 against the threat of oxidative stress damage. In addition to oxidative stress protection, other genes critical to BBB function were selectively altered by the 10 nm nanoAg. These included those associated with clathrin-mediated endocytosis, caveolar invagination, and vesicle trafficking. Surface modification has been reported to facilitate nanosize particles entry into cells using their endocytotic pathways,[30,60−63] and alteration of these genes by the PVP-coated nanoAg in the present study may reflect a stimulation of endocytotic activity. Vascular endothelial growth factor (*Vegfa*), an endothelial mitogen associated with BBB permeability and angiogenesis,[64−68] was marginally but significantly increased by both the 10 nm (1.8 fold) and 75 nm (1.6 fold) PVP-coated nanoAg. PVP in itself has proven angiogenic in both animal models and endothelial cell lines,[68−70] which raises concern given its increased use in medical products such as blood volume extenders[71] and hydrogels used in wound dressings[72] and in brain imaging.[73] Finally, the high affinity glutamate transporter *Slc1a2* was the highest upregulated gene in response to both sizes of PVP-coated nanoAgs and the 10 nm citrate-coated nanoAg. This membrane-bound protein is a critical for clearing L-glutamate from the surrounding interstitial fluid and prevents overexcitation of the neuron.[38] Although glutamate homeostasis has been associated largely with neurons and astrocytes, more recently it has been shown to involve BBB endothelial cells.[74] To explain the high stimulation of this gene in the present study, it should be noted that free radical release has been linked to increased glutamate release[75,76] and impairment of glutamate transport.[77,78] In view of its predominant activation, one might speculate that nanoAg exposure activates a regulatory mechanism that affects glutamate transporters such as *Slc1a2*.

In summary, this study presents cellular and genomic data that indicate a higher bioreactivity for PVP-coated nanoAgs in RBEC4 relative to their citrate-coated counterparts. The smaller size PVP-capped nanoAg was distinctly more active in terms of permeability disruption and affecting cellular and genomic changes associated with oxidative stress, specifically those associated with ARE/NRF2 pathways. Taken together, these data indicate that surface coating, aggregate size, and zeta potential of PVP-coated nanoAg are physicochemical factors that influence nanoAg's bioactivation of RBEC4. Such data sets could prove useful in the future design of safer and more sustainable

nanoAg materials for use by the consumer and in the environment.

■ ASSOCIATED CONTENT

Supporting Information

All techniques are fully described. This material is available free of charge via the Internet at http://pubs.acs.org.

■ AUTHOR INFORMATION

Corresponding Author

*Phone: 919-541-5780. E-mail: veronesi.bellina@epa.gov.

Notes

The authors declare no competing financial interest.

■ ACKNOWLEDGMENTS

Acknowledgements are given to Molly Windsor of SRA International, Inc. for her graphics and excellent illustration. A variety of techniques were used to measure the response of RBEC4 at various times and concentrations and include physicochemical measures (aggregate size and surface charge); high resolution microscopy (confocal, electron microscopy); permeability measures in RBEC4 monolayers using transcellular electrical resistance (TER) recordings; fluorescence-based viability and oxidative stress assays; and genomic evaluation using transfected reporter genes, target gene expression, and global gene expression.

■ REFERENCES

(1) Ahamed, M.; Alsalhi, M. S.; Siddiqui, M. K. Silver nanoparticle applications and human health. *Clin. Chim. Acta* **2010**, *411* (23−24), 1841−1848.

(2) Lem, K. W.; Choudhury, A.; Lakhani, A. A.; Kuyate, P.; Haw, J. R.; Lee, D. S.; Iqbal, Z.; Brumlik, C. J. Use of nanosilver in consumer products. *Recent Pat. Nanotechnol.* **2012**, *6* (1), 60−72.

(3) Som, C.; Wick, P.; Krug, H.; Nowack, B. Environmental and health effects of nanomaterials in nanotextiles and facade coatings. *Environ. Int.* **2011**, *37* (6), 1131−1142.

(4) Faunce, T.; Watal, A. Nanosilver and global public health: International regulatory issues. *Nanomedicine* **2010**, *5* (4), 617−632.

(5) Chaloupka, K.; Malam, Y.; Seifalian, A. M. Nanosilver as a new generation of nanoproduct in biomedical applications. *Trends Biotechnol.* **2010**, *28* (11), 580−588.

(6) Chen, X.; Schluesener, H. J. Nanosilver: A nanoproduct in medical application. *Toxicol. Lett.* **2008**, *176* (1), 1−12.

(7) Nowack, B.; Krug, H. F.; Height, M. 120 Years of nanosilver history: Implications for policy makers. *Environ. Sci. Technol.* **2011**, *45*, 1177−1183.

(8) Liu, J.; Sonshine, D. A.; Shervani, S.; Hurt, R. H. Controlled release of biologically active silver from nanosilver surfaces. *ACS Nano* **2010**, *4* (11), 6903−6913.

(9) Sun, Y.; Gates, B.; Mayers, B.; Xia, Y. Crystalline silver nanowires by soft solution processing. *Nano Lett.* **2002**, *2* (2), 165−168.

(10) Henglein, A.; Giersig, M. Formation of colloidal silver nanoparticles: Capping action of citrate. *J. Phys. Chem. B* **1999**, *103* (44), 9533−9539.

(11) Pastoriza-Santos, I.; Liz-Marzín, L. M. Formation of PVP-protected metal nanoparticles in DMF. *Langmuir* **2002**, *18* (7), 2888−2894.

(12) Tolaymat, T. M.; El Badawy, A. M.; Genaidy, A.; Scheckel, K. G.; Luxton, T. P.; Suidan, M. An evidence-based environmental perspective of manufactured silver nanoparticle in syntheses and applications: A systematic review and critical appraisal of peer-reviewed scientific papers. *Sci. Total Environ.* **2010**, *408* (5), 999−1006.

(13) Itoh, K.; Nakamura, K.; Iijima, M.; Sesaki, H. Mitochondrial dynamics in neurodegeneration. *Trends Cell Biol.* **2013**, *23* (2), 64−71.

(14) Moran, M.; Moreno-Lastres, D.; Marin-Buera, L.; Arenas, J.; Martin, M. A.; Ugalde, C. Mitochondrial respiratory chain dysfunction: Implications in neurodegeneration. *Free Radical Biol. Med.* **2012**, *53* (3), 595−609.

(15) Hirsch, E. C.; Faucheux, B.; Damier, P.; Mouatt-Prigent, A.; Agid, Y. Neuronal vulnerability in Parkinson's disease. *J. Neural Transm., Suppl.* **1997**, *50*, 79−88.

(16) Melo, A.; Monteiro, L.; Lima, R. M.; Oliveira, D. M.; Cerqueira, M. D.; El-Bacha, R. S. Oxidative stress in neurodegenerative diseases: Mechanisms and therapeutic perspectives. *Oxid. Med. Cell. Longevity* **2011**, *2011*, 467180.

(17) Volker, C.; Oetken, M.; Oehlmann, J. The biological effects and possible modes of action of nanosilver. *Rev. Environ. Contam Toxicol.* **2013**, *223*, 81−106.

(18) Carlson, C.; Hussain, S. M.; Schrand, A. M.; Braydich-Stolle, L. K.; Hess, K. L.; Jones, R. L.; Schlager, J. J. Unique cellular interaction of silver nanoparticles: Size-dependent generation of reactive oxygen species. *J. Phys. Chem. B* **2008**, *112* (43), 13608−13619.

(19) Choi, J. E.; Kim, S.; Ahn, J. H.; Youn, P.; Kang, J. S.; Park, K.; Yi, J.; Ryu, D. Y. Induction of oxidative stress and apoptosis by silver nanoparticles in the liver of adult zebrafish. *Aquat. Toxicol.* **2010**, *100* (2), 151−159.

(20) Rahman, M. F.; Wang, J.; Patterson, T. A.; Saini, U. T.; Robinson, B. L.; Newport, G. D.; Murdock, R. C.; Schlager, J. J.; Hussain, S. M.; Ali, S. F. Expression of genes related to oxidative stress in the mouse brain after exposure to silver-25 nanoparticles. *Toxicol. Lett.* **2009**, *187* (1), 15−21.

(21) Ahamed, M.; Posgai, R.; Gorey, T. J.; Nielsen, M.; Hussain, S. M.; Rowe, J. J. Silver nanoparticles induced heat shock protein 70, oxidative stress and apoptosis in Drosophila melanogaster. *Toxicol. Appl. Pharmacol.* **2010**, *242* (3), 263−269.

(22) Abbott, N. J.; Patabendige, A. A.; Dolman, D. E.; Yusof, S. R.; Begley, D. J. Structure and function of the blood-brain barrier. *Neurobiol. Dis.* **2010**, *37* (1), 13−25.

(23) Banks, W. A. Blood-brain barrier as a regulatory interface. *Forum Nutr.* **2010**, *63*, 102−110.

(24) Roux, F.; Couraud, P. O. Rat brain endothelial cell lines for the study of blood-brain barrier permeability and transport functions. *Cell Mol. Neurobiol.* **2005**, *25* (1), 41−58.

(25) Sumi, N.; Nishioku, T.; Takata, F.; Matsumoto, J.; Watanabe, T.; Shuto, H.; Yamauchi, A.; Dohgu, S.; Kataoka, Y. Lipopolysaccharide-activated microglia induce dysfunction of the blood-brain barrier in rat microvascular endothelial cells co-cultured with microglia. *Cell Mol. Neurobiol.* **2010**, *30* (2), 247−253.

(26) Perriere, N.; Demeuse, P.; Garcia, E.; Regina, A.; Debray, M.; Andreux, J. P.; Couvreur, P.; Scherrmann, J. M.; Temsamani, J.; Couraud, P. O.; Deli, M. A.; Roux, F. Puromycin-based purification of rat brain capillary endothelial cell cultures. Effect on the expression of blood-brain barrier-specific properties. *J. Neurochem.* **2005**, *93* (2), 279−289.

(27) Morofuji, Y.; Nakagawa, S.; So, G.; Hiu, T.; Horai, S.; Hayashi, K.; Tanaka, K.; Suyama, K.; Deli, M. A.; Nagata, I.; Niwa, M. Pitavastatin strengthens the barrier integrity in primary cultures of rat brain endothelial cells. *Cell Mol. Neurobiol.* **2010**, *30* (5), 727−735.

(28) Garcia-Garcia, E.; Andrieux, K.; Gil, S.; Kim, H. R.; Le, D. T.; Desmaele, D.; d'Angelo, J.; Taran, F.; Georgin, D.; Couvreur, P. A methodology to study intracellular distribution of nanoparticles in brain endothelial cells. *Int. J. Pharm.* **2005**, *298* (2), 310−314.

(29) Garcia-Garcia, E.; Gil, S.; Andrieux, K.; Desmaele, D.; Nicolas, V.; Taran, F.; Georgin, D.; Andreux, J. P.; Roux, F.; Couvreur, P. A relevant in vitro rat model for the evaluation of blood-brain barrier translocation of nanoparticles. *Cell. Mol. Life Sci.* **2005**, *62* (12), 1400−1408.

(30) Kim, H. R.; Gil, S.; Andrieux, K.; Nicolas, V.; Appel, M.; Chacun, H.; Desmaele, D.; Taran, F.; Georgin, D.; Couvreur, P. Low-density lipoprotein receptor-mediated endocytosis of PEGylated nanoparticles in rat brain endothelial cells. *Cell. Mol. Life Sci.* **2007**, *64* (3), 356−364.

(31) Kim, H. R.; Andrieux, K.; Gil, S.; Taverna, M.; Chacun, H.; Desmaele, D.; Taran, F.; Georgin, D.; Couvreur, P. Translocation of poly(ethylene glycol-co-hexadecyl)cyanoacrylate nanoparticles into rat

brain endothelial cells: Role of apolipoproteins in receptor-mediated endocytosis. *Biomacromolecules.* **2007**, *8* (3), 793−799.
(32) Loeschner, K.; Hadrup, N.; Qvortrup, K.; Larsen, A.; Gao, X.; Vogel, U.; Mortensen, A.; Lam, H. R.; Larsen, E. H. Distribution of silver in rats following 28 days of repeated oral exposure to silver nanoparticles or silver acetate. *Part. Fibre Toxicol.* **2011**, *8*, 18.
(33) Tang, J.; Xiong, L.; Wang, S.; Wang, J.; Liu, L.; Li, J.; Yuan, F.; Xi, T. Distribution, translocation and accumulation of silver nanoparticles in rats. *J. Nanosci. Nanotechnol.* **2009**, *9* (8), 4924−4932.
(34) Reidy, B. Mechanisms of silver nanoparticle release, transformation and toxicity: A critical review of current knowledge and recommendations for future studies and applications. *Materials* **2013**, *6*, 2295−2350.
(35) Lubick, N. Nanosilver toxicity: Ions, nanoparticles—or both? *Environ. Sci. Technol.* **2008**, *42* (23), 8617.
(36) Wijnhoven, S. W. P.; Peijnenburg, W. J. G. M.; Herberts, C. A.; Hagens, W. I.; Oomen, A. G.; Heugens, E. H. W.; Roszek, B.; Bisschops, J.; Gosens, I.; Van De Meent, D.; Dekkers, S.; De Jong, W. H.; van Zijverden, M.; Sips, A. J. A. M.; Geertsma, R. E. Nano-silver − A review of available data and knowledge gaps in human and environmental risk assessment. *Nanotoxicology* **2009**, *3* (2), 109−138.
(37) Kittler, S.; Greulich, C.; Gebauer, J. S.; Diendorf, J.; Treuel, L.; Ruiz, L.; Gonzalez-Calbet, J. M.; Vallet-Regi, M.; Zellner, R.; Koller, M.; Epple, M. The influence of proteins on the dispersability and cell-biological activity of silver nanoparticles. *J. Mater. Chem.* **2010**, *20* (3), 512−518.
(38) Kanai, Y.; Clemencon, B. F.; Simonin, A.; Leuenberger, M.; Lochner, M.; Weisstanner, M.; Hediger, M. A. The SLC1 high-affinity glutamate and neutral amino acid transporter family. *Mol. Aspects Med.* **2013**, *34* (2−3), 108−120.
(39) Lu, W.; Tan, Y. Z.; Jiang, X. G. Establishment of coculture model of blood-brain barrier in vitro for nanoparticle's transcytosis and toxicity evaluation. *Yaoxue Xuebao* **2006**, *41* (4), 296−304.
(40) Oh, P.; Borgstrom, P.; Witkiewicz, H.; Li, Y.; Borgstrom, B. J.; Chrastina, A.; Iwata, K.; Zinn, K. R.; Baldwin, R.; Testa, J. E.; Schnitzer, J. E. Live dynamic imaging of caveolae pumping targeted antibody rapidly and specifically across endothelium in the lung. *Nat. Biotechnol.* **2007**, *25* (3), 327−337.
(41) Alyaudtin, R. N.; Reichel, A.; Lobenberg, R.; Ramge, P.; Kreuter, J.; Begley, D. J. Interaction of poly(butylcyanoacrylate) nanoparticles with the blood-brain barrier in vivo and in vitro. *J. Drug Targeting* **2001**, *9* (3), 209−221.
(42) Koch, A. M.; Reynolds, F.; Merkle, H. P.; Weissleder, R.; Josephson, L. Transport of surface-modified nanoparticles through cell monolayers. *ChemBioChem* **2005**, *6* (2), 337−345.
(43) Youssef, J.; Archibald, P.; Jiang, C.; Emmanuel, S.; Didier, B. Influence of surface charge and inner composition of porous nanoparticles to cross blood-brain barrier in vitro. *Int. J. Pharm.* **2007**, *344*, 103−109.
(44) Lockman, P. R.; Koziara, J. M.; Mumper, R. J.; Allen, D. D. Nanoparticle surface charges alter blood-brain barrier integrity and permeability. *J. Drug Targeting* **2004**, *12* (9−10), 635−641.
(45) Huwyler, J.; Cerletti, A.; Fricker, G.; Eberle, A. N.; Drewe, J. By-passing of P-glycoprotein using immunoliposomes. *J. Drug Targeting* **2002**, *10* (1), 73−79.
(46) Choi, O.; Hu, Z. Size dependent and reactive oxygen species related nanosilver toxicity to nitrifying bacteria. *Environ. Sci. Technol.* **2008**, *42* (12), 4583−4588.
(47) El Badawy, A. M.; Silva, R. G.; Morris, B.; Scheckel, K. G.; Suidan, M. T.; Tolaymat, T. M. Surface charge-dependent toxicity of silver nanoparticles. *Environ. Sci. Technol.* **2011**, *45* (1), 283−287.
(48) Nel, A. E.; Madler, L.; Velegol, D.; Xia, T.; Hoek, E. M.; Somasundaran, P.; Klaessig, F.; Castranova, V.; Thompson, M. Understanding biophysicochemical interactions at the nano-bio interface. *Nat. Mater.* **2009**, *8* (7), 543−557.
(49) Karaman DS FAU - Desai, D.; Desai, D. F.; Senthilkumar, R.; Johansson, E. M.; Ratts, N.; Oden, M.; Eriksson, J.; Sahlgren, C.; Sahlgren, C.; Toivola, D. M.; Rosenholm, J. M. Shape engineering vs organic modification of inorganic nanoparticles as a tool for enhancing cellular internalization. *Nanoscale Res. Lett.* **2012**, *7* (1), 358.
(50) Oberdorster, G.; Oberdorster, E.; Oberdorster, J. Nanotoxicology: An emerging discipline evolving from studies of ultrafine particles. *Environ. Health Perspect.* **2005**, *113* (7), 823−839.
(51) Nel, A.; Xia, T.; Madler, L.; Li, N. Toxic potential of materials at the nanolevel. *Science* **2006**, *311* (5761), 622−627.
(52) Kreyling, W. G.; Semmler-Behnke, M.; Moller, W. Ultrafine particle-lung interactions: Does size matter? *J. Aerosol Med.* **2006**, *19* (1), 74−83.
(53) Huynh, K. A.; Chen, K. L. Aggregation kinetics of citrate and polyvinylpyrrolidone coated silver nanoparticles in monovalent and divalent electrolyte solutions. *Environ. Sci. Technol.* **2011**, *45* (13), 5564−5571.
(54) El Badawy, A. M.; Luxton, T. P.; Silva, R. G.; Scheckel, K. G.; Suidan, M. T.; Tolaymat, T. M. Impact of environmental conditions (pH, ionic strength, and electrolyte type) on the surface charge and aggregation of silver nanoparticles suspensions. *Environ. Sci. Technol.* **2010**, *44* (4), 1260−1266.
(55) Caballero-Diaz, E.; Pfeiffer, C.; Kastl, L.; Rivera-Gil, P.; Simonet, B.; Valcírcel, M.; Jinez-Lamana, J.; Laborda, F.; Parak, W. J. The toxicity of silver nanoparticles depends on their uptake by cells and thus on their surface chemistry. *Part. Part. Syst. Charact.* **2013**, *30* (12), 1079−1085.
(56) Bryan, H. K.; Olayanju, A.; Goldring, C. E.; Park, B. K. The Nrf2 cell defense pathway: Keap1-dependent and -independent mechanisms of regulation. *Biochem. Pharmacol.* **2013**, *85* (6), 705−717.
(57) Venugopal, R.; Jaiswal, A. K. Nrf1 and Nrf2 positively and c-Fos and Fra1 negatively regulate the human antioxidant response element-mediated expression of NAD(P)H:quinone oxidoreductase1 gene. *Proc. Natl. Acad. Sci. U.S.A.* **1996**, *93* (25), 14960−14965.
(58) Tada, M.; Yokosuka, O.; Fukai, K.; Chiba, T.; Imazeki, F.; Tokuhisa, T.; Saisho, H. Hypermethylation of NAD(P)H: Quinone oxidoreductase 1 (NQO1) gene in human hepatocellular carcinoma. *J. Hepatol.* **2005**, *42* (4), 511−519.
(59) Calkins, M. J.; Johnson, D. A.; Townsend, J. A.; Vargas, M. R.; Dowell, J. A.; Williamson, T. P.; Kraft, A. D.; Lee, J. M.; Li, J.; Johnson, J. A. The Nrf2/ARE pathway as a potential therapeutic target in neurodegenerative disease. *Antioxid. Redox Signaling* **2009**, *11* (3), 497−508.
(60) Zhao, F.; Zhao, Y.; Liu, Y.; Chang, X.; Chen, C.; Zhao, Y. Cellular uptake, intracellular trafficking, and cytotoxicity of nanomaterials. *Small* **2011**, *7* (10), 1322−1337.
(61) Smith, M. W.; Gumbleton, M. Endocytosis at the blood-brain barrier: from basic understanding to drug delivery strategies. *J. Drug Targeting* **2006**, *14* (4), 191−214.
(62) Wohlfart, S.; Gelperina, S.; Kreuter, J. Transport of drugs across the blood-brain barrier by nanoparticles. *J. Controlled Release* **2012**, *161*, 264−273.
(63) Banks, W. A.; Kastin, A. J.; Akerstrom, V. HIV-1 protein gp120 crosses the blood-brain barrier: Role of adsorptive endocytosis. *Life Sci.* **1997**, *61* (9), L119−L125.
(64) Argaw, A. T.; Gurfein, B. T.; Zhang, Y.; Zameer, A.; John, G. R. VEGF-mediated disruption of endothelial CLN-5 promotes blood-brain barrier breakdown. *Proc. Natl. Acad. Sci. U.S.A.* **2009**, *106* (6), 1977−1982.
(65) Boveri, M.; Berezowski, V.; Price, A.; Slupek, S.; Lenfant, A. M.; Benaud, C.; Hartung, T.; Cecchelli, R.; Prieto, P.; Dehouck, M. P. Induction of blood-brain barrier properties in cultured brain capillary endothelial cells: Comparison between primary glial cells and C6 cell line. *Glia* **2005**, *51* (3), 187−198.
(66) Davis, B.; Tang, J.; Zhang, L.; Mu, D.; Jiang, X.; Biran, V.; Vexler, Z.; Ferriero, D. M. Role of vasodilator stimulated phosphoprotein in VEGF induced blood-brain barrier permeability in endothelial cell monolayers. *Int. J. Dev. Neurosci.* **2010**, *28* (6), 423−428.
(67) Hawkins, B. T.; Sykes, D. B.; Miller, D. S. Rapid, reversible modulation of blood-brain barrier P-glycoprotein transport activity by vascular endothelial growth factor. *J. Neurosci.* **2010**, *30* (4), 1417−1425.
(68) Zhang, Z. G.; Zhang, L.; Jiang, Q.; Zhang, R.; Davies, K.; Powers, C.; Bruggen, N.; Chopp, M. VEGF enhances angiogenesis and promotes

blood-brain barrier leakage in the ischemic brain. *J. Clin. Invest* **2000**, *106* (7), 829−838.
(69) Kang, K.; Lim, D. H.; Choi, I. H.; Kang, T.; Lee, K.; Moon, E. Y.; Yang, Y.; Lee, M. S.; Lim, J. S. Vascular tube formation and angiogenesis induced by polyvinylpyrrolidone-coated silver nanoparticles. *Toxicol. Lett.* **2011**, *205*, 227−234.
(70) Zagami, C. J.; Beart, P. M.; Wallis, N.; Nagley, P.; O'Shea, R. D. Oxidative and excitotoxic insults exert differential effects on spinal motoneurons and astrocytic glutamate transporters: Implications for the role of astrogliosis in amyotrophic lateral sclerosis. *Glia* **2009**, *57* (2), 119−135.
(71) Singh, R.; Singh, D. Radiation synthesis of PVP/alginate hydrogel containing nanosilver as wound dressing. *J. Mater. Sci. Mater. Med.* **2012**, *23* (11), 2649−2658.
(72) Seth, D.; Choudhury, S. R.; Pradhan, S.; Gupta, S.; Palit, D.; Das, S.; Debnath, N.; Goswami, A. Nature-inspired novel drug design paradigm using nanosilver: Efficacy on multi-drug-resistant clinical isolates of tuberculosis. *Curr. Microbiol.* **2011**, *62* (3), 715−726.
(73) Serganova, I.; Mayer-Kukuck, P.; Huang, R.; Blasberg, R. Molecular imaging: Reporter gene imaging. *Handb. Exp. Pharmacol.* **2008**, *185 Pt 2*, 167−223.
(74) Helms, H. C.; Madelung, R.; Waagepetersen, H. S.; Nielsen, C. U.; Brodin, B. In vitro evidence for the brain glutamate efflux hypothesis: Brain endothelial cells cocultured with astrocytes display a polarized brain-to-blood transport of glutamate. *Glia* **2012**, *60* (6), 882−893.
(75) Gilman, S. C.; Bonner, M. J.; Pellmar, T. C. Effect of oxidative stress on excitatory amino acid release by cerebral cortical synaptosomes. *Free Radical Biol. Med.* **1993**, *15* (6), 671−675.
(76) Pellegrini-Giampietro, D. E.; Cherici, G.; Alesiani, M.; Carla, V.; Moroni, F. Excitatory amino acid release and free radical formation may cooperate in the genesis of ischemia-induced neuronal damage. *J. Neurosci.* **1990**, *10* (3), 1035−1041.
(77) Keller, J. N.; Mark, R. J.; Bruce, A. J.; Blanc, E.; Rothstein, J. D.; Uchida, K.; Waeg, G.; Mattson, M. P. 4-Hydroxynonenal, an aldehydic product of membrane lipid peroxidation, impairs glutamate transport and mitochondrial function in synaptosomes. *Neuroscience* **1997**, *80* (3), 685−696.
(78) Pedersen, W. A.; Cashman, N. R.; Mattson, M. P. The lipid peroxidation product 4-hydroxynonenal impairs glutamate and glucose transport and choline acetyltransferase activity in NSC-19 motor neuron cells. *Exp. Neurol.* **1999**, *155* (1), 1−10.